Z. Phys. C 62, 357–365 (1994)

ZEITSCHRIFT
FÜR PHYSIK C

Study of hard scattering processes in multihadron production from $\gamma\gamma$ collisions at LEP

DELPHI Collaboration

P. Abreu[20], W. Adam[7], T. Adye[37], E. Agasi[30], R. Aleksan[39], G.D. Alekseev[14], P. Allport[21], S. Almehed[23], F.M.L. Almeida Junior[47], S.J. Alvsvaag[4], U. Amaldi[7], A. Andreazza[27], P. Antilogus[24], W.-D. Apel[15], R.J. Apsimon[37], Y. Arnoud[39], B. Åsman[44], J.-E. Augustin[18], A. Augustinus[30], P. Baillon[7], P. Bambade[18], F. Barao[20], R. Barate[12], G. Barbiellini[46], D.Y. Bardin[14], G.J. Barker[34], A. Baroncelli[40], O. Barring[7], J.A. Barrio[25], W. Bartl[50], M.J. Bates[37], M. Battaglia[13], M. Baubillier[22], K.-H. Becks[52], M. Begalli[36], P. Beilliere[6], Yu. Belokopytov[42], P. Beltran[9], A.C. Benvenuti[5], M. Berggren[18], D. Bertrand[2], F. Bianchi[45], M. Bigi[45], M.S. Bilenky[14], P. Billoir[22], J. Bjarne[23], D. Bloch[8], J. Blocki[51], S. Blyth[34], V. Bocci[38], P.N. Bogolubov[14], T. Bolognese[39], M. Bonesini[27], W. Bonivento[27], P.S.L. Booth[21], G. Borisov[42], C. Bosio[40], B. Bostjancic[43], S. Bosworth[34], O. Botner[48], B. Bouquet[18], C. Bourdarios[18], T.J.V. Bowcock[21], M. Bozzo[11], S. Braibant[2], P. Branchini[40], K.D. Brand[35], R.A. Brenner[13], H. Briand[22], C. Bricman[2], L. Brillault[22], R.C.A. Brown[7], P. Bruckman[16], J.-M. Brunet[6], A. Budziak[16], L. Bugge[32], T. Buran[32], A. Buys[7], J.A.M.A. Buytaert[7], M. Caccia[27], M. Calvi[27], A.J. Camacho Rozas[41], R. Campion[21], T. Camporesi[7], V. Canale[38], K. Cankocak[44], F. Cao[2], F. Carena[7], P. Carrilho[47], L. Carroll[21], R. Cases[49], M.V. Castillo Gimenez[49], A. Cattai[7], F.R. Cavallo[5], L. Cerrito[38], V. Chabaud[7], A. Chan[1], M. Chapkin[42], Ph. Charpentier[7], J. Chauveau[22], P. Checchia[35], G.A. Chelkov[14], L. Chevalier[39], P. Chliapnikov[42], V. Chorowicz[22], J.T.M. Chrin[49],V. Cindro[43], P. Collins[34], J.L. Contreras[18], R. Contri[11], E. Cortina[49], G. Cosme[18], F. Couchot[18], H.B. Crawley[1], D. Crennell[37], G. Crosetti[11], J. Cuevas Maestro[33], S. Czellar[13], E. Dahl-Jensen[28], J. Dahm[52], B. Dalmagne[18], M. Dam[32], G. Damgaard[28], G. Darbo[11], E. Daubie[2], A. Daum[15], P.D. Dauncey[7], M. Davenport[7], J. Davies[21], W. Da Silva[22], C. Defoix[6], P. Delpierre[26], N. Demaria[34], A. De Angelis[7], H. De Boeck[2], W. De Boer[15], S. De Brabandere[2], C. De Clerq[2], M.D.M. De Fez Laso[49], C. De La Vaissiere[22], B. De Lotto[46], A. De Min[27], L. De Paula[47], H. Dijkstra[7], L. Di Ciaccio[38], F. Djama[8], J. Dolbeau[6], M. Donszelmann[7], K. Doroba[51], M. Dracos[7], J. Drees[52], M. Dris[31], Y. Dufour[7], F. Dupont[12], D. Edsall[1], L.-O. Eek[48], R. Ehret[15], T. Ekelof[48], G. Ekspong[44], A. Elliot Peisert[7], M. Elsing[52], J.-P. Engel[8], N. Ershaidat[22], M. Espirito Santo[20], D. Fassouliotis[31], M. Feindt[7], A. Fenyuk[42], A. Ferrer[49], T.A. Filippas[31], A. Firestone[1], H. Foeth[7], E. Fokitis[31], F. Fontanelli[11], K.A.J. Forbes[21], F. Formenti[7], J.-L. Fousset[26], S. Francon[24], B. Franek[37], P. Frenkiel[6], D.C. Fries[15], A.G. Frodesen[4], R. Fruhwirth[50], F. Fulda-Quenzer[18], H. Furstenau[7], J. Fuster[7], D. Gamba[45], M. Gandelman[17], C. Garcia[49], J. Garcia[41], C. Gaspar[7], U. Gasparini[35], Ph. Gavillet[7], E.N. Gazis[31], J.-P. Gerber[8], P. Giacomelli[7], D. Gillespie[7], R. Gokieli[51], B. Golob[43], V.M. Golovatyuk[14], J.J. Gomez Y Cadenas[7], G. Gopal[37], L. Gorn[1], M. Gorski[51], V. Gracco[11], F. Grard[2], E. Graziani[40], G. Grosdidier[18], B. Grossetete[22], P. Gunnarsson[44], J. Guy[37], U. Haedinger[15], F. Hahn[52], M. Hahn[44], S. Hahn[52], S. Haider[30], Z. Hajduk[16], A. Hakansson[23], A. Hallgren[48], K. Hamacher[52], G. Hamel De Monchenault[39], W. Hao[30], F.J. Harris[34], V. Hedberg[23], R. Henriques[20], J.J. Hernandez[49], J.A. Hernando[49], P. Herquet[2], H. Herr[7], T.L. Hessing[21], C.O. Higgins[21], E. Higon[49], H.J. Hilke[7], T.S. Hill[1], S.D. Hodgson[34], T. Hofmokl[51], S.-O. Holmgren[44], P.J. Holt[34], D. Holthuizen[30], P.F. Honore[6], M. Houlden[21], K. Huet[2], K. Hultqvist[44], P. Ioannou[3], P.-S. Iversen[4], J.N. Jackson[21], R. Jacobsson[44], P. Jalocha[16], G. Jarlskog[23], P. Jarry[39], B. Jean-Marie[18], E.K. Johansson[44], M. Jonker[7], L. Jonsson[23], P. Juillot[8], M. Kaiser[15], G. Kalkanis[3], G. Kalmus[37], F. Kapusta[22], M. Karlsson[44], E. Karvelas[9], S. Katsanevas[3], E.C. Katsoufis[31], R. Keranen[7], B.A. Khomenko[14], N.N. Khovanski[14], B. King[21], N.J. Kjaer[28], H. Klein[7], A. Klovning[4], P. Kluit[30], A. Koch-Mehrin[52], J.H. Koehne[15], B. Koene[30], P. Kokkinias[9], M. Koratzinos[32], K. Korcyl[16], A.V. Korytov[14], V. Kostioukhine[42], C. Kourkoumelis[3], O. Kouznetsov[14], P.H. Kramer[52], M. Krammer[50], C. Kreuter[15], J. Krolikowski[51], I. Kronkvist[23], W. Krupinski[16], W. Kucewicz[16], K. Kulka[48], K. Kurvinen[13], C. Lacasta[49], C. Lambropoulos[9], J.W. Lamsa[1], L. Lanceri[46], P. Langefeld[52], V. Lapin[42], I. Last[21], J.-P. Laugier[39], R.Lauhakangas[13], G. Leder[50], F. Ledroit[12], R. Leitner[29], Y. Lemoigne[39], J. Lemonne[2], G. Lenzen[52], V. Lepeltier[18], J.M. Levy[8], E. Lieb[52], D. Liko[50], J. Lindgren[13], R. Lindner[52], A. Lipniacka[18], I. Lippi[35], B. Loerstad[23], M. Lokajicek[10], J.G. Loken[34], A. Lopez-Fernandez[7], M.A. Lopez Aguera[41], M. Los[30], D. Loukas[9], J.J. Lozano[49], P. Lutz[6], L. Lyons[34], G. Maehlum[15], J. Maillard[6], A. Maio[20], A. Maltezos[9], F. Mandl[50], J. Marco[41], B. Marechal[47], M. Margoni[35], J.-C. Marin[7], C. Mariotti[40], A. Markou[9], T. Maron[52], S. Marti[49], C. Martinez-Rivero[41], F. Martinez-Vidal[49], F. Matorras[41], C. Matteuzzi[27], G. Matthiae[38], M. Mazzucato[35], M. Mc Cubbin[21], R. Mc Kay[1], R. Mc Nulty[21], J. Medbo[48], C. Meroni[27], W.T. Meyer[1], M. Michelotto[35], E. Migliore[45], I. Mikulec[50], L. Mirabito[24], W.A. Mitaroff[50], G.V. Mitselmakher[14], U. Mjoernmark[23], T. Moa[45], R. Moeller[28], K. Moenig[7], M.R. Monge[11], P. Morettini[11], H. Mueller[15], W.J. Murray[37], B. Muryn[16], G. Myatt[34], F. Naraghi[12], F.L. Navarria[5], P. Negri[27], S. Nemecek[10], W. Neumann[52], N. Neumeister[50], R. Nicolaidou[3], B.S. Nielsen[28], V. Nikolaenko[42], P.E.S. Nilsen[4], P. Niss[45], A. Nomerotski[35], N. Novak[10], V. Obraztsov[42], A.G. Olshevski[14], R. Orava[13], A. Ostankov[42],

K. Osterberg[13], A. Ouraou[39], P. Paganini[18], M. Paganoni[27], R. Pain[22], H. Palka[16], Th.D. Papadopoulou[31], L. Pape[7], F. Parodi[11], A. Passeri[40], M. Pegoraro[35], J. Pennanen[13], L. Peralta[20], V. Perevozchikov[42], H. Pernegger[50], M. Pernicka[50], A. Perrotta[5], C. Petridou[46], A. Petrolini[11], G. Piana[11], F. Pierre[39], M. Pimenta[20], S. Plaszczynski[18], O. Podobrin[15], M.E. Pol[17], G. Polok[16], P. Poropat[46], V. Pozdniakov[14], M. Prest[46], P. Privitera[38], A. Pullia[27], D. Radojicic[34], S. Ragazzi[27], H. Rahmani[31], P.N. Ratoff[19], A.L. Read[32], M. Reale[52], P. Rebecchi[18], N.G. Redaelli[27], M. Regler[50], D. Reid[7], P.B. Renton[34], L.K. Resvanis[3], F. Richard[18], J. Richardson[21], J. Ridky[10], G. Rinaudo[45], A. Romero[45], I. Roncagliolo[11], P. Ronchese[35], E.I. Rosenberg[1], E. Rosso[7], P. Roudeau[18], T. Rovelli[5], W. Ruckstuhl[30], V. Ruhlmann-Kleider[39], A. Ruiz[41], H. Saarikko[13], Y. Sacquin[39], G. Sajot[12], J. Salt[49], J. Sanchez[25], M. Sannino[11], S. Schael[7], H. Schneider[15], M.A.E. Schyns[52], G. Sciolla[45], F. Scuri[46], A.M. Segar[34], A. Seitz[15], R. Sekulin[37], M. Sessa[46], R. Seufert[15], R.C. Shellard[36], I. Siccama[30], P. Siegrist[39], S. Simonetti[11], F. Simonetto[35], A.N. Sisakian[14], G. Skjevling[32], G. Smadja[39,24], O. Smirnova[14], G.R. Smith[37], R. Sosnowski[51], D. Souza-Santos[36], T. Spassov[20], E. Spiriti[40], S. Squarcia[11], H. Staeck[52], C. Stanescu[40], S. Stapnes[32], G. Stavropoulos[9], F. Stichelbaut[7], A. Stocchi[18], J. Strauss[50], J. Straver[7], R. Strub[8], B. Stugu[4], M. Szczekowski[51], M. Szeptycka[51], P. Szymanski[51], T. Tabarelli[27], O. Tchikilev[42], G.E. Theodosiou[9], Z. Thome[47], A. Tilquin[26], J. Timmermans[30], V.G. Timofeev[14], L.G. Tkatchev[14], T. Todorov[8], D.Z. Toet[30], A. Tomaradze[2], B. Tome[20], E. Torassa[45], L. Tortora[40], D. Treille[7], W. Trischuk[7], G. Tristram[6], C. Troncon[27], A. Tsirou[7], E.N. Tsyganov[14], M.-L. Turluer[39], T. Tuuva[13], I.A. Tyapkin[22], M. Tyndel[37], S. Tzamarias[21], B. Ueberschaer[52], S. Ueberschaer[52], O. Ullaland[7], V. Uvarov[42], G. Valenti[5], E. Vallazza[7], J.A. Valls Ferrer[49], C. Vander Velde[2], G.W. Van Apeldoorn[30], P. Van Dam[30], M. Van Der Heijden[30], W.K. Van Doninck[2], J. Van Eldik[30], P. Vaz[7], G. Vegni[27], L. Ventura[35], W. Venus[37], F. Verbeure[2], M. Verlato[35], L.S. Vertogradov[14], D. Vilanova[39], P. Vincent[24], L. Vitale[46], E. Vlasov[42], A.S. Vodopyanov[14], M. Vollmer[52], M. Voutilainen[13], V. Vrba[10], H. Wahlen[52], C. Walck[44], F. Waldner[46], A. Wehr[52], M. Weierstall[52], P. Weilhammer[7], A.M. Wetherell[7], J.H. Wickens[2], M. Wielers[15], G.R. Wilkinson[34], W.S.C. Williams[34], M. Winter[8], G. Wormser[18], K. Woschnagg[48], A. Zaitsev[42], A. Zalewska[16], D. Zavrtanik[43], E. Zevgolatakos[9], N.I. Zimin[14], M. Zito[39], D. Zontar[43], R. Zuberi[34], G. Zumerle[35]

[1] Ames Laboratory and Department of Physics, Iowa State University, Ames, IA 50011, USA
[2] Physics Department, University Instelling Antwerpen, Universiteitsplein 1, B-2610 Wilrijk, Belgium, and IIHE, ULB-VUB, Pleinlaan 2, B-1050 Brussels, Belgium, and Faculté des Sciences, Université de l'Etat Mons, Avenue Maistriau 19, B-7000 Mons, Belgium
[3] Physics Laboratory, University of Athens, Solonos Str. 104, GR-10680 Athens, Greece
[4] Department of Physics, University of Bergen, Allégaten 55, N-5007 Bergen, Norway
[5] Dipartimento di Fisica, Università di Bologna and INFN, Via Irnerio 46, I-40126 Bologna, Italy
[6] Collège de France, Laboratoire de Physique Corpusculaire, IN2P3-CNRS, F-75231 Paris Cedex 05, France
[7] CERN, CH-1211 Geneva 23, Switzerland
[8] Centre de Recherche Nucléaire, IN2P3, CNRS/ULP, BP20, F-67037 Strasbourg Cedex, France
[9] Institute of Nuclear Physics, N.C.S.R. Demokritos, P.O. Box 60228, GR-15310 Athens, Greece
[10] FZU, Institute of Physics of the C.A.S. High Energy Physics Division, Na Slovance 2, CS-180 40, Praha 8, Czechoslovakia
[11] Dipartimento di Fisica, Università di Genova and INFN, Via Dodecaneso 33, I-16146 Genova, Italy
[12] Institut des Sciences Nucléaires, IN2P3-CNRS, Université de Grenoble 1, F-38026 Grenoble, France
[13] Research Institute for High Energy Physics, SEFT, P.O. Box 9, FIN-00014 University of Helsinki, Finland
[14] Joint Institute for Nuclear Research, Dubna, Head Post Office, P.O. Box 79, 101 000 Moscow, Russian Federation
[15] Institut für Experimentelle Kernphysik, Universität Karlsruhe, Postfach 6980, D-76128 Karlsruhe, Germany
[16] High Energy Physics Laboratory, Institute of Nuclear Physics, Ul. Kawiory 26a, PL-30055 Krakow 30, Poland
[17] Centro Brasileiro de Pesquisas Fisicas, rua Xavier Sigaud 150, RJ-22290 Rio de Janeiro, Brazil
[18] Université de Paris-Sud, Laboratoire de l'Accélérateur Linéaire, IN2P3-CNRS, Bât. 200, F-91405 Orsay, France
[19] School of Physics and Materials, University of Lancaster, Lancaster LA1 4YB, UK
[20] LIP, IST, FCUL, Av. Elias Garcia, 14, 1°, P-1000 Lisboa Codex, Portugal
[21] Department of Physics, University of Liverpool, P.O. Box 147, Liverpool L69 3BX, UK
[22] LPNHE, IN2P3-CNRS, Universités Paris VI et VII, Tour 33 (RdC), 4 place Jussieu, F-75252 Paris Cedex 05, France
[23] Department of Physics, University of Lund, Sölvegatan 14, S-22363 Lund, Sweden
[24] Université Claude Bernard de Lyon, IPNL, IN2P3-CNRS, F-69622 Villeurbanne Cedex, France
[25] Universidad Complutense, Avda. Complutense s/n, E-28040 Madrid, Spain
[26] Université d'Aix, Marseille II, CPP, IN2P3-CNRS, F-13288 Marseille Cedex 09, France
[27] Dipartimento di Fisica, Università di Milano and INFN, Via Celoria 16, I-20133 Milan, Italy
[28] Niels Bohr Institute, Blegdamsvej 17, DK-2100 Copenhagen 0, Denmark
[29] NC, Nuclear Centre of MFF, Charles University, Areal MFF, V Holesovickach 2, CS-180 00, Praha 8, Czechoslovakia
[30] NIKHEF-H, Postbus 41882, 1009 DB Amsterdam, The Netherlands
[31] National Technical University, Physics Department, Zografou Campus, GR-15773 Athens, Greece
[32] Physics Department, University of Oslo, Blindern, N-1000 Oslo 3, Norway
[33] Dpto. Fisica, Univ. Oviedo, C/P. Jimenez Casas, S/N, E-33006 Oviedo, Spain
[34] Department of Physics, University of Oxford, Keble Road, Oxford OX1 3RH, UK
[35] Dipartimento di Fisica, Università di Padova and INFN, Via Marzolo 8, I-35131 Padua, Italy
[36] Depto. de Fisica, Pontificia Univ. Católica, C.P. 38071, RJ-22453 Rio de Janeiro, Brazil
[37] Rutherford Appleton Laboratory, Chilton, Didcot OX11 OQX, UK
[38] Dipartimento di Fisica, Università di Roma II and INFN, Tor Vergata, I-00173 Rome, Italy
[39] Centre d'Etude de Saclay, DSM/DAPNIA, F-91191 Gif-sur-Yvette Cedex, France
[40] Istituto Superiore di Sanità, Ist. Naz. di Fisica Nucl. (INFN), Viale Regina Elena 299, I-00161 Rome, Italy

[41] C.E.A.F.M., C.S.I.C., Univ. Cantabria, Avda. los Castros, E-39006 Santander, Spain
[42] Inst. for High Energy Physics, Serpukov P.O. Box 35, Protvino, (Moscow Region), Russian Federation
[43] J. Stefan Institute and Department of Physics, University of Ljubljana, Jamova 39, SI-61000 Ljubljana, Slovenia
[44] Fysikum, Stockholm University, Box 6730, S-113 85 Stockholm, Sweden
[45] Dipartimento di Fisica Sperimentale, Università di Torino and INFN, Via P. Giuria 1, I-10125 Turin, Italy
[46] Dipartimento di Fisica, Università di Trieste and INFN, Via A. Valerio 2, I-34127 Trieste, Italy and Istituto di Fisica, Università di Udine, I-33100 Udine, Italy
[47] Univ. Federal do Rio de Janeiro, C.P. 68528 Cidade Univ., Ilha do Fundão BR-21945-970 Rio de Janeiro, Brazil
[48] Department of Radiation Sciences, University of Uppsala, P.O. Box 535, S-751 21 Uppsala, Sweden
[49] IFIC, Valencia-CSIC, and D.F.A.M.N., U. de Valencia, Avda. Dr. Moliner 50, E-46100 Burjassot (Valencia), Spain
[50] Institut für Hochenergiephysik, Österr. Akad. d. Wissensch., Nikolsdorfergasse 18, A-1050 Vienna, Austria
[51] Inst. Nuclear Studies and University of Warsaw, Ul. Hoza 69, PL-00681 Warsaw, Poland
[52] Fachbereich Physik, University of Wuppertal, Postfach 100 127, D-42097 Wuppertal, Germany

Received: 17 January 1994

Abstract. The production of multihadronic states in $\gamma\gamma$ collisions at LEP has been studied with the DELPHI detector. The analyzed data correspond to an integrated luminosity of about 32 pb^{-1}, collected in the LEP runs of 1990–1992. Minimum bias data and a sample of events with jets at high p_T have been selected under the requirement that no scattered electron or positron is observed. The two data sets have been compared to Monte Carlo predictions. The non-perturbative contribution described by the vector meson dominance Model and direct $q\bar{q}$ production from pointlike photons described by the quark parton model were found to be insufficient to reproduce the data. It has been necessary to include a third interaction component, which is due to perturbative hard scattering of the partonic constituents of the photon. Several parametrisations of the quark and gluon densities of the photon have been tested. The interplay with the cut in jet transverse momentum, which is necessary for the separation of the perturbative and non-perturbative regions, is discussed. The data favour parametrisations with rather soft partonic content of the photon.

1 Introduction

The reaction $e^+e^- \to e^+e^- X$, where X is a multihadronic system, has been intensively studied at PEP [1], at PETRA [2] and more recently at KEK [3] and LEP [4]. Emphasis has been on collisions of quasi-real photons at relatively high $\gamma\gamma$ centre of mass energy, in order to stay away from the two-photon resonance region. These data are qualitatively described by a model [5] combining the vector meson dominance model (VDM) and the quark parton model (QPM). As illustrated in Fig. 1a and b, these models describe the interaction through bound-state vector mesons and through direct coupling, respectively. However, the data do exceed the QPM prediction of particle momenta transverse to the $\gamma\gamma$ axis p_T above 1.5 GeV/c [2]. This observation suggests the presence of QCD subprocesses and offers the possibility to constrain the quark and gluon density of the photon experimentally. The picture of hard scattering subprocesses, shown in Fig. 1c and d, relies on high four-momentum transfers or high p_T^2, probing the structure of one or both photons and resolving them into their partonic constituents.

The fully non-perturbative term is described through VDM as the diffractive scattering of vector mesons. The other contributions are treated using Leading Order QCD factorisation: a hard scattering subprocess fixes the dominant scale p_T^2, taken also as the factorisation scale, and the photon participates via direct coupling to quarks, or via a quark or a gluon produced through a QCD evolution starting from a bound state or a perturbative $q\bar{q}$

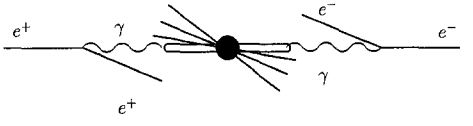

a) Nonperturbative contribution (VDM)

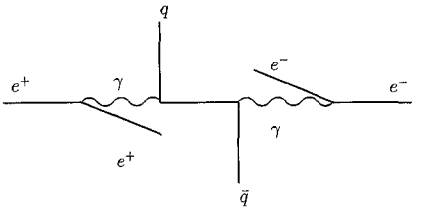

b) Direct photon contribution (QPM)

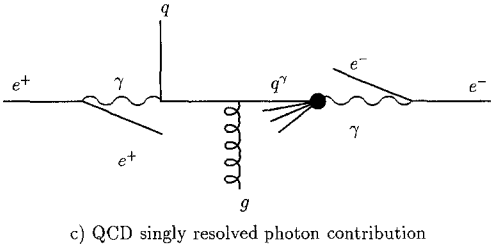

c) QCD singly resolved photon contribution

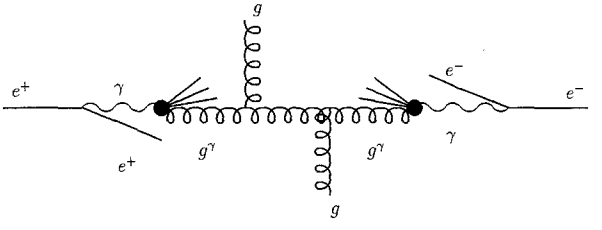

d) QCD doubly resolved photon contribution

Fig. 1a–d. Processes contributing to the production of multihadron states in photon-photon collisions

pair state. According to the Drees classification [6] there are three terms: the direct term of Fig. 1b, the singly resolved photon contribution of Fig. 1c, and the doubly resolved contribution of Fig. 1d.

Most secondary particles from two-photon events go into the low-angle region of the detector, and only some of the particles of the final system are seen. The resolved photons produce remnant or beam pipe jets which may mix with decay products of the low-p_T central system. The presence of jets of (moderately) high p_T at large angles forms a signature for the isolation of the hard scattering subprocesses against the dominant diffractive dissociation contribution. The quark and gluon densities of the photon could in principle be obtained from deep inelastic $e\gamma$ scattering data at relatively low Q^2, where Q^2 is the absolute squared mass of the photon associated to the detected lepton. However, the consistency of such a procedure is still an open problem: since the subprocesses are perturbative, a cut at low transverse momentum, $p_T^{\min}$, has to be specified, which in the present study is much larger than the mass of the virtual photon, whereas Q^2 and $(p_T^{min}/c)^2$ ought to be of the same order to obtain useful densities. Therefore, various sets of quark and gluon densities in the photon, with corresponding $p_T^{\min}$ parameter, have been tested directly against the present data. LEP energies are in principle favoured for such studies, since the parton densities inside a photon are peaked at low x and jet production approximately probes the region $x \simeq 2p_T/\langle W_{\gamma\gamma}\rangle$, where $\langle W_{\gamma\gamma}\rangle$ is the average invariant mass of the $\gamma\gamma$ system, which is of the order of 10% of the e^+e^- centre of mass energy. In practice, due to trigger conditions, acceptance cuts or jet search requirements, the average parton momentum fraction of the photon is within the range 0.2–0.3.

In the following the VDM parameters will be fixed according to the results of previous experiments and the remnant jets will be produced at zero angle with respect to the two-photon centre of mass axis. Although this approach is not expected to lead to a complete discrimination between parametrizations, it should indicate the distinctive requirements for a successful parametrization. In particular, hard parton distributions will produce more high-p_T jets in the central region, while soft distributions lead to more energy deposition in the remnant jets.

Data taken with the DELPHI detector during the years 1990–1992 have been used for an analysis of hadronic final states produced in $\gamma\gamma$ collisions at a mean value of the absolute squared virtual photon masses, as evaluated by Monte Carlo simulation, of about 0.12 $(\mathrm{GeV}/c^2)^2$.

2 The DELPHI detector

A detailed description of the DELPHI detector can be found in [7]. Only the components of the detector relevant to the analysis of the $\gamma\gamma$ events (tracking and electromagnetic calorimetry) are briefly described here.

- The main tracking system is a time projection chamber (TPC). The cylindrical TPC has an inner radius of 35 cm, an outer radius of 111 cm and is 268 cm long in the beam direction. Tracks of charged particles are measured in the TPC with a resolution of about 230 μm in the $R\phi$ plane (transverse to the beam) and about 0.9 mm along the beam direction.

- The inner detector (ID) is a cylindrical drift chamber with jet-chamber geometry surrounded by 5 cylindrical MWPC layers. The space covered by the ID extends from 12 cm to 28 cm in the radial direction and ± 40 cm in the beam direction. The coordinate resolution in the jet chamber is about 90 μm in the $R\phi$ plane. The layers of proportional chambers provide a fast trigger and z-coordinate information and resolve left/right ambiguities in the jet section.

- In the barrel region the tracking system is completed by the outer detector (OD) at a radius of about 200 cm. Five layers of drift tubes measure $R\phi$ coordinates with a resolution of about 110 μm and three layers also provide a z-measurement with a resolution of about 2 cm.

- Tracking in the forward-backward regions ($11° < \theta < 33°$ and $147° < \theta < 169°$) is complemented with two pairs of additional drift chambers (FCA and FCB). The FCA modules are mounted directly on the endplates of the TPC. Each side consists of three pairs of wire planes, rotated by 120° with respect to each other in order to resolve ambiguities. The precision of FCA is about 150 μm in x and y. The FCB detectors are mounted in front of the endcap electromagnetic calorimeter. Each detector consists of 12 wire planes arranged with a geometry similar to FCA. The precision of FCB is about 120 μm in x and y.
- Electromagnetic energy is measured in the forward-backward regions by a lead glass calorimeter (FEMC) consisting of 4522 lead blocks in each endcap. They cover the angular regions $10° < \theta < 36.5°$ and $143.5° < \theta < 170°$. The angular resolution of the FEMC as measured for 45 GeV electrons is about 0.3°.

- The small-angle tagger (SAT) is a calorimeter consisting of alternating layers of lead sheets and scintillating fibres, covering polar angles from 2.5° to 7.7° on both sides. It was used for luminosity measurements and for the suppression of two-photon events with a scattered electron within its angular range (anti-tagging), and it contributed also to the measurement of the total visible energy of each event.

The hadron calorimeter (HAC) has been used to assist in the discrimination of $\gamma\gamma$ events against the background from Z decays, but information from this detector was not included in the final event analysis. In the barrel region, electromagnetic energy is measured by a high density projection chamber (HPC). Due to the relatively high threshold of the HPC, the low energy photons in the $\gamma\gamma$ events gave a small contribution to the overall energy. They were included in the jet reconstruction algorithm [8].

The quality of the trigger system is very important in $\gamma\gamma$ data taking, due to the low multiplicity of the final state and the low particle momenta. The main components of the DELPHI trigger for this analysis are the

coincidence of ID and OD signals, the coincidence of signals in the FCA and FCB, and the TPC subtriggers. The neutral component contributes negligibly to the $\gamma\gamma$ trigger rate. A determination of the trigger efficiency is described in the next section.

3 Event selection

The multiplicity and total energy of the charged particles in an event formed the basic criteria for event preselection. Charged particle tracks were accepted if the following criteria were met:

- momentum above 0.4 GeV/c;
- polar angle in the range $20° < \theta < 160°$;
- radial projection of the impact parameter relative to the interaction point below 4 cm;
- projection of the impact parameter along the beam direction below 8 cm;
- relative error on momentum measurement less than 100%.

All calorimetric information has been included in the event selection for discrimination against background from Z decays. Taking into account the sensitivity, stability and noise performance of the calorimeters, the following thresholds were chosen: 0.5 GeV for the FEMC and HPC, 1.5 GeV for the HAC and 2.0 GeV for the SAT. Data have been compared with Monte Carlo results for forward-backward oriented hadronic Z events in order to check the quality of the simulation for charged and neutral particles. All distributions were found to be in good agreement.

The following criteria were used for the selection of two-photon events:

1. at least 4 charged particles in the event;
2. total energy of the charged particles below 12 GeV;
3. total visible energy below 20 GeV;
4. invariant mass of the hadronic system in the range 3–13 GeV/c^2;
5. total transverse momentum below 2.5 GeV/c;
6. net charge of the observed charged particles not more than one unit.

Criterion 1 selects hadronic final states. Criteria 2 and 3 suppress Z background. Criteria 3 and 5 constrain the experimental conditions to explicit anit-tagging and add to the suppression of Z background. The lower limit in criterion 4 suppresses the resonance region of the $\gamma\gamma$ interaction and most of the beam-gas events, while the upper limit further reduces the Z background. Criterion 6 removes the majority of the remaining beam-gas events.

Events fulfilling the criteria 1–6 constitute the minimum bias sample, in the following referred to as sample I. This sample was obtained from data taken in 1991 and 1992. Secondly, a more restricted sample of events with high-p_T jets was defined (sample II). In addition to the cuts mentioned above, two jets with $p_T > 1.75$ GeV/c and polar angles between 40° and 140° were required. The jets were defined using the Lund cluster algorithm [8] in the visible centre of mass, optimized for a two-jet search with the QPM Monte Carlo. This sample was extracted from all data taken in 1990–1992.

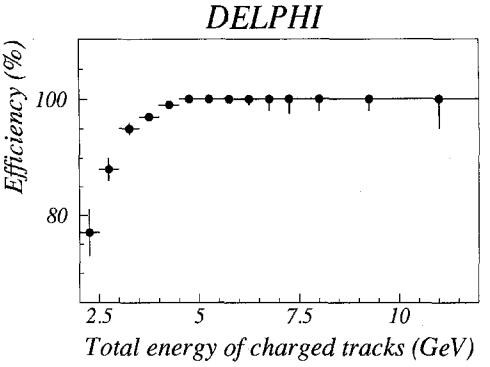

Fig. 2. Trigger efficiency vs total visible energy of charged particles for $\gamma\gamma$ events

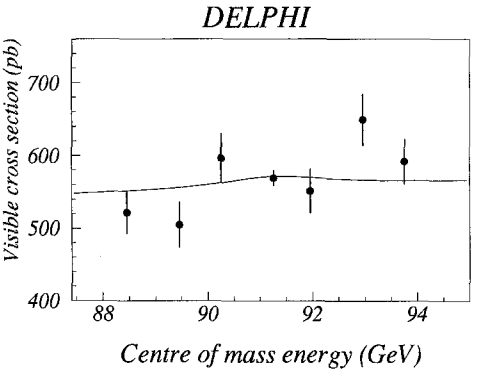

Fig. 3. Visible cross section of selected events as a function of centre of mass energy

The forward-backward regions of the detector play the most important role in the $\gamma\gamma$ trigger. Information on all trigger components was recorded for each event. The single-track trigger efficiency was calculated by use of the redundancy among independent triggers. Figure 2 shows the trigger efficiency in the 1991 and 1992 runs for sample I data as a function of the total visible energy of charged particles.

Convolution of the energy dependence of the trigger efficiency with the distribution of the total energy of the charged particles leads to the following trigger efficiencies: $95.5^{+0.8}_{-1.5}$% for sample I and $99.0^{+0.5}_{-1.0}$% for sample II.

The cross section for events fulfilling the selection criteria was calculated for each LEP energy point. A fit of the energy dependence of the cross section was performed on the 1991 data as an additional check, in order to obtain an estimate of the visible cross section from Z background and from $\gamma\gamma$ events. Cahn's formula [9], which takes into account dominant radiative effects of Z decays only, is sufficient in this case of low statistics and a low contamination of the sample with Z decays, and was combined with a linear term describing the two photon contribution.

The fit (Fig. 3) applied to the 1991 data selected by criteria 1-6 (sample I) gives the following cross sections:

$\sigma^{\exp}_{\gamma\gamma(\mathrm{I})} = 554 \pm 23$ pb and $\sigma^{\exp}_{Z(\mathrm{I})} = 23 \pm 37$ pb.

For sample II the values are:

$\sigma^{\exp}_{\gamma\gamma(\mathrm{II})} = 10.9 \pm 4.0$ pb and $\sigma^{\exp}_{Z(\mathrm{II})} = 2.0 \pm 6.1$ pb.

A Monte Carlo simulation including both $q\bar{q}$ and $\tau^+\tau^-$ events was used to check the visible cross section due to Z background. The results are compatible with the cross sections extracted from the fit above:

$\sigma^{MC}_{qq(\mathrm{I})} = 7.0 \pm 0.7$ pb, $\sigma^{MC}_{\tau\tau(\mathrm{I})} = 0.14 \pm 0.06$ pb

for the minimum bias sample;

$\sigma^{MC}_{qq(\mathrm{II})} = 0.2 \pm 0.1$ pb, $\sigma^{MC}_{\tau\tau(\mathrm{II})} = 0.02 \pm 0.01$ pb

for the events with two high-p_T jets.

These estimates from simualtion were used for the subtraction of Z background. A selected sample of events originating far from the interaction point ($10\,\mathrm{cm} < |z| < 20\,\mathrm{cm}$) was used to estimate the cross section of the beam-gas background:

$\sigma_{bg(\mathrm{I})} = 3.0 \pm 0.5$ pb and $\sigma_{bg(\mathrm{II})} = 0.0 \pm 0.1$ pb.

Other sources (virtual Compton process, tau pairs from $\gamma\gamma$ interactions) give much lower contributions, in agreement with previous studies.

4 Models

Both event samples have been compared with model predictions.

The Vector Meson Dominance Model was used to describe the fully non-perturbative regime. The $\gamma\gamma$ cross section is given by:

$$\sigma_{\gamma\gamma}(W^2, Q^2, P^2) = F_{\mathrm{VDM}}(Q^2) F_{\mathrm{VDM}}(P^2) \left[A + \frac{B}{W}\right] \quad (1)$$

where W is the invariant mass of the two-photon system and Q^2 and P^2 are the absolute squared masses of the two virtual photons. We have taken $A = 275$ nb and $B = 300$ nb · GeV [10]. These values are about 10% larger than in the standard Rosner formula [11]. This type of parametrization has already been used by previous experiments [12, 13]. The quantity F_{VDM} is the generalized VDM form factor [14]:

$$F_{\mathrm{VDM}}(Q^2) = \sum_{V=\rho,\omega,\phi} r_V \frac{1 + Q^2/4m_V^2}{(1 + Q^2/m_V^2)^2} + \frac{0.22}{1 + Q^2/m_0^2} \quad (2)$$

where m_V denotes a vector meson mass and r_V is related to the vector meson coupling to the photon. The last term in (2), where the value $m_0 = 1.4$ GeV was used, describes the contribution from the radial excitations of vector mesons. The multihadronic final state was generated as a $q\bar{q}$ pair, with a quark distribution $d\sigma/dp_T^2 \simeq \exp(-5p_T^2)$ in the $\gamma\gamma$ centre of mass system, fragmented according to JETSET 7.3 [8]. The parameter σ_q in JETSET, describing the width of the Gaussian distribution of primary hadrons within a jet, was set to 450 MeV/c in order to take into account the bound-state origin of the quarks [2].

The quark parton model generator was used to describe the interaction term due to direct photon-quark coupling, analogous to the QED process $ee \to ee\mu\mu$.

Within the QCD multi-jet component, the central p_T^2 of the hard scattering subprocess, which is always greater than the perturbative cut-off $(p_T^{\min})^2$, probes the structure of one photon in singly resolved processes, or both photons in doubly resolved processes [15]. In this approach the two photons need to be quasi-real. This is indeed the case, since their average absolute squared masses, as obtained from Monte Carlo, are of the order of 0.1 $(\mathrm{GeV}/c^2)^2$, much lower than $(p_T^{\min}/c)^2$. The quarks and gluons are emitted from a photon through QCD evolution, starting from either a point-like or a bound state coupling, whose separation implies the use of another momentum transfer or p_T^0 cut-off [16] at the first quark pair creation level. Since the existing quark and gluon parametrizations do not allow such a distinction, the approach in the present study has been that the outgoing partons will give rise to high-p_T jets, while the spectator partons produce remnant jets. The latter were generated along the direction of the incoming quasi-real photons. This point deserves further study, together with the p_T^0 cut, because of the efffect on the detected particles from remnant jets. Many partonic density functions of the photon are available, but since they are extracted from deep inelastic $e\gamma$ scattering at high Q^2, they sometimes cannot be used for hard scattering at relatively low p_T^2/c^2. Only Leading Order parametrisations have been considered.

A priori, each parametrisation is associated to a special value of $p_T^{\min}$, constrained by the description of the visible total cross section. The following parton density functions [17], starting from Q^2 larger or equal to 1 GeV^2/c^4, have been used: the parametrisations due to Duke and Owens (DO) [18], Drees and Grassie (DG) [15], Levy, Abramowicz and Charchula (LAC1) [19] and Gordon and Storrow (GS) [20]. The main differences among these sets stem from their behaviour at low x.

5 Results and discussion

After background subtraction and efficiency corrections, the following values were obtained for the visible cross section of the two samples of $\gamma\gamma$ events:

$\sigma^{\exp}_{\gamma\gamma(\mathrm{I})} = 573 \pm 5\,(\mathrm{stat}) \pm 19\,(\mathrm{syst})$ pb

$\sigma^{\exp}_{\gamma\gamma(\mathrm{II})} 12.8 \pm 0.7\,(\mathrm{stat}) \pm 0.4\,(\mathrm{syst})$ pb.

The quoted systematic errors are the quadratic sum of uncertainties in trigger efficiency (1%), in selection efficiency (1%) and in the background estimation (3%).

The Monte Carlo generated events were processed by the detector simulation program and were submitted to the same selection procedure as the experimental data. The calculations of thrust and jet transverse momentum were performed in the $\gamma\gamma$ visible centre-of-mass system. The resulting QPM and VDM predictions for sample I are:

$$\sigma^{\mathrm{QPM}}_{\gamma\gamma\,(\mathrm{I})} = 34.5 \pm 1.0\,(\mathrm{stat})\ \mathrm{pb}$$

$$\sigma^{\mathrm{VDM}}_{\gamma\gamma\,(\mathrm{I})} = 287.2 \pm 4.7\,(\mathrm{stat})\,{}^{+140}_{-\ 57}\,(\mathrm{theory})\ \mathrm{pb}$$

with a theoretical error coming from various predictions found in the literature. Neglecting for the moment the large systematic error, their incoherent sum is not sufficient to describe the experimental visible cross section of sample I. One may of course try to force agreement with experiment without inclusion of QCD subprocesses by tuning VDM. However, as already shown by the AMY collaboration [3] and as evident from the present data, it is not possible to explain data in the region of high-p_T jets by such tuning of VDM.

Use of the sample of events with two jets at high p_T (sample II) eliminates the large uncertainty from the VDM cross section. The size of the VDM contribution is small in this sample. In addition, the influence of errors from the determination of the $p_T^{\min}$ cut in the QCD model becomes strongly reduced for sample I, assuming VDM contribution to be 287.2 pb as given by the Monte Carlo. The systematic uncertainty in the VDM cross section for data sample II is estimated as $^{+0.35}_{-0.14}$ pb. The model cross sections for sample II are:

$$\sigma^{\mathrm{QPM}}_{\gamma\gamma\,(\mathrm{II})} = 3.9 \pm 0.5\,(\mathrm{stat})\ \mathrm{pb} \quad \text{and}$$

$$\sigma^{\mathrm{VDM}}_{\gamma\gamma\,(\mathrm{II})} = 0.7 \pm 0.2\,(\mathrm{stat})\ \mathrm{pb}\,.$$

Thus, the result from the two-component model,

$$\sigma^{\mathrm{VDM+QPM}}_{\gamma\gamma\,(\mathrm{II})} = 4.6 \pm 0.6\,(\mathrm{stat})\ \mathrm{pb}\,,$$

is appreciably smaller than the experimental cross section for sample II events.

The next step has been to add the QCD component, with several parametrization functions. For each parametrization, the cut $p_T^{\min}$ was determined by the requirement that the three-component model should reproduce the measured cross section for sample I. With these values of $p_T^{\min}$, the three-component model cross section was then determined using the event selection criteria of sample II. The results for four different parton density parametrisations are:

$$\sigma^{\mathrm{DO}}_{\gamma\gamma\,(\mathrm{II})} = \ 7.9 \pm 0.6\,(\mathrm{stat})\ \mathrm{pb}$$

$$\sigma^{\mathrm{DG}}_{\gamma\gamma\,(\mathrm{II})} = \ 9.4 \pm 0.7\,(\mathrm{stat})\ \mathrm{pb}$$

$$\sigma^{\mathrm{LAC1}}_{\gamma\gamma\,(\mathrm{II})} = 12.2 \pm 1.2\,(\mathrm{stat})\ \mathrm{pb}$$

$$\sigma^{\mathrm{GS}}_{\gamma\gamma\,(\mathrm{II})} = 13.3 \pm 0.9\,(\mathrm{stat})\ \mathrm{pb}\,.$$

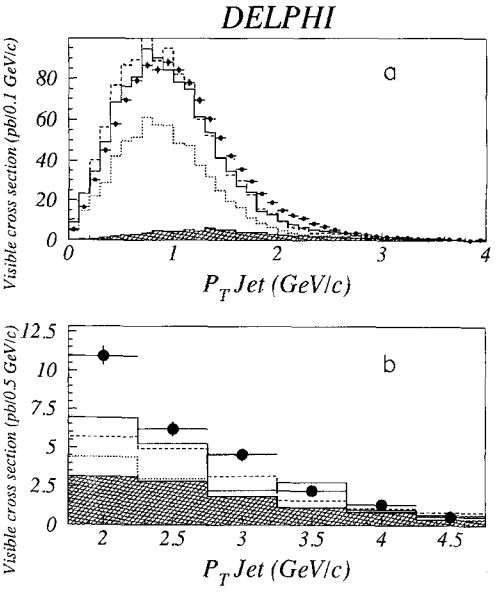

Fig. 4. The distributions of jet transverse momentum for sample I (**a**) and sample II (**b**) in comparison with Monte Carlo predictions. Hatched area: QPM only; dots: QPM + VDM; full line: QPM + VDM + DG ($p_T^{\min} = 1.45$ GeV/c); dashed line: QPM + VDM + DO ($p_T^{\min} = 1.22$ GeV/c)

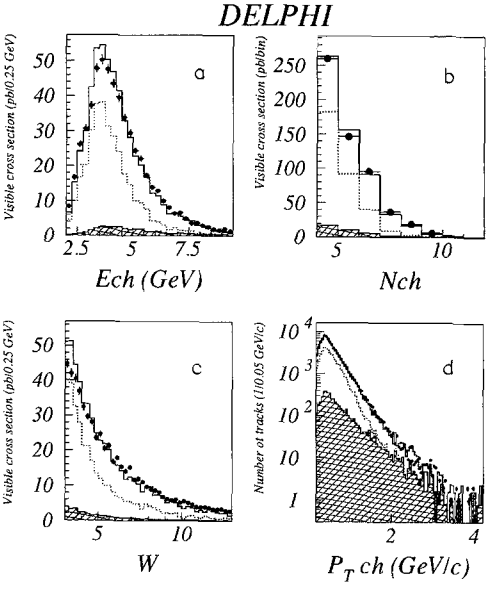

Fig. 5a–d. Distributions of event variables for sample I in comparison with Monte Carlo predictions. QPM – hatched area, QPM + VDM – dots, QPM + VDM + GS ($p_T^{\min} = 1.83$ GeV/c) – full line. **a** Total energy of charged particles, **b** charged multiplicity, **c** invariant mass of the $\gamma\gamma$ system and **d** transverse track momentum

Clearly, the DG and DO parametrisations are too soft and fail to describe the data in the region of high-p_T jets. The LAC1 and GS parton densities give a quantitatively correct prediction. The same conclusion follows from comparison of the distributions of various event variables with the respective Monte Carlo results. Already at the level of sample I, it is found that the DG and the DO parametrizations disagree with the data in the region of the tails of the jet p_T and invariant mass of the multi-

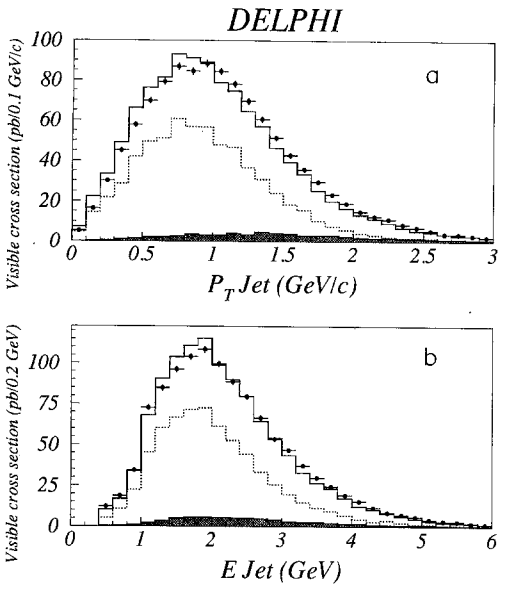

Fig. 6. Transverse momentum (**a**) and energy of the reconstructed jets (**b**) for sample I in comparison with Monte Carlo predictions. QPM - hatched area, QPM + VDM - dots, QPM + VDM + GS ($p_T^{\min} = 1.83$ GeV/c) - full line

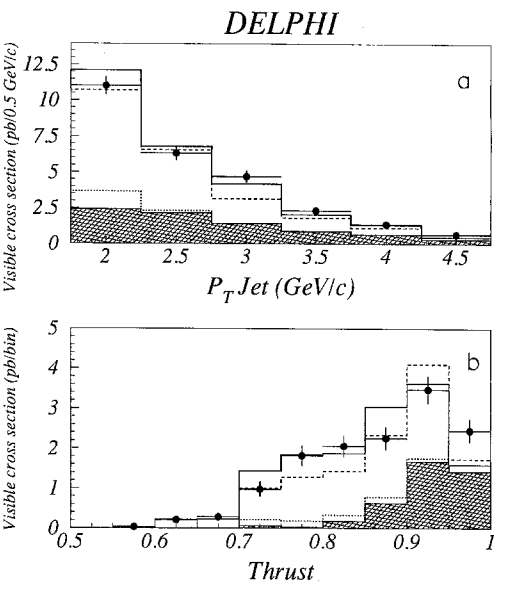

Fig. 8. Transverse momentum of jets (**a**) and the event thrust (**b**) for sample II in comparison with Monte Carlo predictions. QPM - hatched area, QPM + VDM - dots, QPM + VDM + GS ($p_T^{\min} = 1.83$ GeV/c) - full line and QPM + VDM + LAC1 ($p_T^{\min} = 2.22$ GeV/c) - dashed line

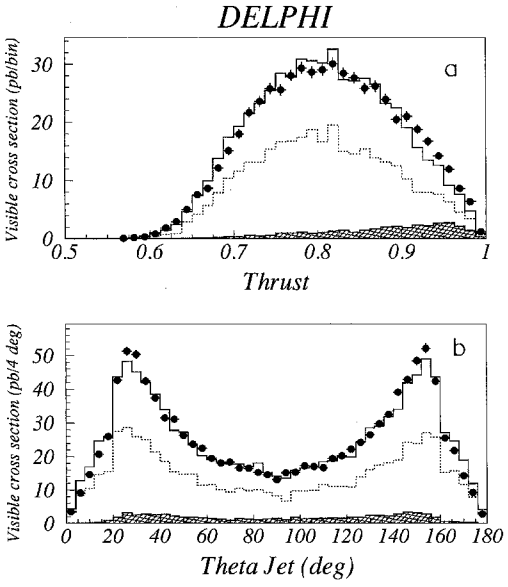

Fig. 7. Event thrust (**a**) and polar angle of the jets (**b**) for sample I in comparison with Monte Carlo predictions. QPM - hatched area, QPM + VDM - dots, QPM + VDM + GS ($p_T^{\min} = 1.83$ GeV/c) - full line

hadronic system distributions. As a consequence of the procedure adopted here, these parametrizations lead to very small cross sections for sample II for any $p_T^{\min}$. This is illustrated by Fig. 4. In fact, parton distributions peaked at very low x mainly lead to low-p_T jets carrying only a small fraction of the two-photon invariant mass, which implies a small high-p_T jet visible cross section. The mixing of central particles and particles from remnant jets is quantified through the thrust variable. The GS and LAC1 parametrizations produce reasonable agreement in most of the distributions (Figs. 5–8). The differences between the GS and LAC1 predictions are very small. Further studies are underway concerning the effect of the treatment of remnant jets on the photon structure description.

If the three-component model is considered as proven, a reduction in the uncertainty on the size of the VDM contribution can be attempted. For both data samples, the correlation can be determined between the cut $p_T^{\min}$ and a rescaling factor of VDM at which the model cross sections agree with the data. In the case of the GS parametrisation, only sample I exhibits a high sensitivity: a $\pm 45\%$ variation in the VDM scaling factor implies a corresponding $\pm 20\%$ one in $p_T^{\min}$. Nevertheless sample II constrains $p_T^{\min}$ around the central value. The LAC1 parametrisation gives similar results.

6 Conclusions

We have studied multihadron production in two-photon collisions at LEP. A three-component model which includes QCD hard scattering subprocesses is needed to describe the data. Rather soft parametrisations of the partonic content of the photon are preferred, although differences in the behaviour at small x remain, in broad agreement with recent AMY results [21]. Further studies of effects related to the simulation treatment of remnant and central jets are continuing.

Acknowledgements. We are greatly indebted to our technical collaborators and to the funding agencies for their support in building and operating the DELPHI detector, and to the members of the CERN-SL Division for the excellent performance of the LEP collider.

References

1. TPC/2γ Coll., H. Aihara et al.: Phys. Rev. Lett. 58 (1987) 97
2. PLUTO Coll., Ch. Berger et al.: Phys. Lett. B149 (1984) 421; TASSO Coll., M. Althoff et al.: Z. Phys. C31 (1986) 527; CELLO Coll., H.-J. Behrend et al.: Z. Phys. C51 (1991) 365
3. AMY Coll., R. Tanaka et al.: Phys. Lett. B277 (1992) 215
4. ALEPH Coll., D. Buskulic et al.: Phys. Lett. B313 (1993) 509; OPAL Coll., R. Akers et al.: CERN-PPE/93-156, Z. Phys. C (1993)
5. V.M. Budnev, I.F. Ginzburg, G.V. Meledin, V.G. Serbo: Phys. Rep. 15C (1975) 181
6. M. Drees, R.M. Godbole: Nucl. Phys. B339 (1990) 355
7. DELPHI Coll., P. Aarnio et al.: Nucl. Instrum. Methods A303 (1991) 233
8. T. Sjostrand, PYTHIA 5.6 and JETSET 7.3., CERN-TH/6488-92
9. R.N. Cahn: Phys. Rev. D36 (1987) 2666
10. I.F. Ginzburg, V.G. Serbo: Phys. Lett. B109 (1982) 231
11. J. Rosner: NBL Report 17522 (1972) 316
12. TPC/Two-Gamma Coll., H. Aihara et al.: Phys. Rev. D41 (1990) 2667
13. PLUTO Coll., Ch. Berger et al.: Z. Phys. C26 (1984) 353
14. S.J. Sakurai, D. Schildknecht: Phys. Lett. B41 (1972) 489
15. M. Drees, K. Grassie: Z. Phys. C28 (1985) 451
16. J.K. Storrow: In: Proc. 9th Int. Workshop on Photon-Photon Collisions, p. 147, San Diego 1992. D.O. Caldwell, H.P. Paar (eds.). Singapore: World Scientific 1993
17. H. Plothow-Besch, PDFLIB: A library of all available parton density functions of the nucleon, the pion and the corresponding α_s calculations. CERN-PPE/92-123
18. D.W. Duke, J.F. Owens: Phys. Rev. D26 (1982) 1600
19. H. Abramowicz, K. Charchula, A. Levy: Phys. Lett. B269 (1991) 458
20. L.E. Gordon, J.K. Storrow: MC-TH 91-29 (1991)
21. R. Tanaka: In: Proc. 9th Int. Workshop on Photon-Photon Collisions, p. 87. San Diego 1992. D.O. Caldwell, H.P. Paar (eds.). Singapore: World Scientific 1993